



**HAL**  
open science

## Propagation of equatorial noise to low altitudes: decoupling from the magnetosonic mode

O. Santolík, Michel Parrot, F. Němec

► **To cite this version:**

O. Santolík, Michel Parrot, F. Němec. Propagation of equatorial noise to low altitudes: decoupling from the magnetosonic mode. *Geophysical Research Letters*, 2016, 43, pp.6694-6704. 10.1002/2016GL069582 . insu-01340021

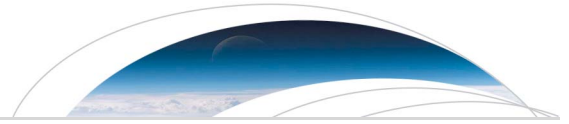
**HAL Id: insu-01340021**

**<https://insu.hal.science/insu-01340021>**

Submitted on 21 Nov 2016

**HAL** is a multi-disciplinary open access archive for the deposit and dissemination of scientific research documents, whether they are published or not. The documents may come from teaching and research institutions in France or abroad, or from public or private research centers.

L'archive ouverte pluridisciplinaire **HAL**, est destinée au dépôt et à la diffusion de documents scientifiques de niveau recherche, publiés ou non, émanant des établissements d'enseignement et de recherche français ou étrangers, des laboratoires publics ou privés.



## RESEARCH LETTER

10.1002/2016GL069582

## Key Points:

- Equatorial noise has been observed under geomagnetically disturbed conditions by the DEMETER spacecraft at a low altitude of 700 km
- Superposition of spectral lines from distant sources; Downward propagation both below and above the local proton cyclotron frequency
- The identified mode is decoupled from the low-frequency magnetosonic mode; A cutoff prevents the waves from propagation to the ground

## Correspondence to:

O. Santolík,  
os@ufa.cas.cz

## Citation:

Santolík, O., M. Parrot, and F. Němec (2016), Propagation of equatorial noise to low altitudes: Decoupling from the magnetosonic mode, *Geophys. Res. Lett.*, 43, 6694–6704, doi:10.1002/2016GL069582.

Received 12 MAY 2016

Accepted 15 JUN 2016

Accepted article online 17 JUN 2016

Published online 4 JUL 2016

## Propagation of equatorial noise to low altitudes: Decoupling from the magnetosonic mode

O. Santolík<sup>1,2</sup>, M. Parrot<sup>3</sup>, and F. Němec<sup>2</sup>

<sup>1</sup>Department of Space Physics, Institute of Atmospheric Physics CAS, Prague, Czechia, <sup>2</sup>Faculty of Mathematics and Physics, Charles University, Prague, Czechia, <sup>3</sup>LPC2E/CNRS, Orleans, France

**Abstract** Equatorial noise (often phenomenologically described as magnetosonic waves in the literature) is a natural electromagnetic emission, which is generated by instability of ion distributions and which can interact with electrons in the Van Allen radiation belts. We use multicomponent electromagnetic measurements of the DEMETER spacecraft to investigate if equatorial noise propagates inward down to the Earth. Analysis of a selected event recorded under disturbed geomagnetic conditions shows that equatorial noise can be observed at an altitude of 700 km, while propagating radially downward as a superposition of spectral lines from different distant sources observed at frequencies both below and above the local proton cyclotron frequency. Changes in the local ion composition encountered by the waves during their inward propagation disconnect the identified wave mode from the low-frequency magnetosonic mode. The local ion composition also induces a cutoff which prevents the waves from propagating down to the ground.

### 1. Introduction

Natural electromagnetic emissions of equatorial noise [Russell *et al.*, 1970; Gurnett, 1976] are receiving increased attention because of their possible importance for electron dynamics in the radiation belts [Horne *et al.*, 2007; Li *et al.*, 2014; Bortnik *et al.*, 2015; Shprits, 2016; Walker *et al.*, 2015a; Ma *et al.*, 2016]. These emissions are composed of a complex system of many spectral lines with spacing ranging from a few hertz to a few tens of hertz, linked to ion cyclotron frequencies in local or distant sources [Gurnett, 1976; Santolík *et al.*, 2002a; Ma *et al.*, 2014]. Superposed rising tone quasiperiodic structures can also occasionally occur [Fu *et al.*, 2014; Boardsen *et al.*, 2014; Němec *et al.*, 2015b].

Equatorial noise is frequently observed within a latitudinal range of about 10° from the geomagnetic equator [Santolík *et al.*, 2004; Němec *et al.*, 2005, 2006; Posch *et al.*, 2015; Hrbáčková *et al.*, 2015], although occasional off-equatorial observations have also been reported [Tsurutani *et al.*, 2014; Zhima *et al.*, 2015]. It occurs at all local times, both outside and inside the plasmopause, at radial distances between 2 and 8 Earth radii ( $R_E$ ) [Ma *et al.*, 2013; Posch *et al.*, 2015; Xiao *et al.*, 2015; Němec *et al.*, 2013, 2015a; Hrbáčková *et al.*, 2015]. Its frequencies are usually found between the proton cyclotron frequency and the lower hybrid frequency [Němec *et al.*, 2005, 2015a; Ma *et al.*, 2013; Boardsen *et al.*, 1992]. This frequency range is in agreement with the prevailing wave generation model at proton Bernstein modes close to proton cyclotron harmonics from unstable proton ring distributions [Meredith *et al.*, 2008; Balikhin *et al.*, 2015; Min and Liu, 2016] and subsequent propagation in the extraordinary mode [Walker *et al.*, 2015b]. This mode exists below the lower hybrid frequency for wave vectors perpendicular to the geomagnetic field.

Emissions of equatorial noise are often referred to as magnetosonic waves in the literature [e.g., Perraut *et al.*, 1982; Laakso *et al.*, 1990; Horne *et al.*, 2000]. However, the same mode name is traditionally used for compressional Alfvén waves at frequencies well below the ion cyclotron frequency [Stix, 1992]. The phenomenological extension of the mode name of magnetosonic waves to equatorial noise at much higher frequencies may therefore be a source of confusion. This extension was, according to Perraut *et al.* [1982], linked to the observations of extraordinary and right-handed polarization of equatorial noise, the same as for the traditional low-frequency magnetosonic mode. This is, in theory, substantiated for a hypothetical case of a purely hydrogen plasma, where the wave mode of equatorial noise is coupled to the low-frequency magnetosonic mode by a smooth transition of the refractive index. Equatorial noise is also coupled to the whistler mode, without any restriction for the plasma composition, and these emissions are therefore also naturally referred to as whistler mode waves in a part of the existing literature [e.g., Russell *et al.*, 1970; Gurnett, 1976; Santolík *et al.*, 2002a; Němec *et al.*, 2005].

Consistent with observations of spectral lines generated by sources at different radial distances from the Earth, radial component of wave propagation has been identified [Santolík *et al.*, 2004; Němec *et al.*, 2013; Xiao *et al.*, 2015]. The waves may propagate radially outward [Walker *et al.*, 2015b] but hypothetically also toward the Earth and reach thus low altitudes. In the case of inward propagation of equatorial noise we would expect that waves generated above the proton cyclotron frequency in the outer regions would travel toward steeply increasing geomagnetic field, and therefore, their frequency might become lower than the local proton cyclotron frequency. This scenario can explain recent results of Boardesen *et al.* [2016], who found equatorial noise below the local proton cyclotron frequency in 8.3% of their events, based on mass processing of the Van Allen Probes survey data using an automated mode identification procedure. However, local generation or even upward propagation from sources below the spacecraft could not be excluded in their case because detailed spectra and wave propagation properties have not been analyzed for these events.

In the present letter we try to answer two open questions: (1) Does equatorial noise propagate from distant sources down to low altitudes and to the Earth? (2) What are its frequency spectra and wave mode in this case? For this purpose we use multicomponent electromagnetic measurements of the low-orbiting DEMETER spacecraft and we present results of a detailed analysis of a selected event with a clear line structure observed under disturbed geomagnetic conditions. We show (1) that equatorial noise can be observed at an altitude of 700 km with a radially downward propagation. We also show that (2) the observed emission is formed by superposition of spectral lines from different distant sources occurring at frequencies both below and above the local proton cyclotron frequency. The observed wave mode is induced by the local plasma containing multiple ion species. It effectively decouples equatorial noise from the low-frequency magnetosonic mode. It also prevents the waves from their further propagation down to the ground. In section 2 of this letter we briefly describe the data set and show the results of a case study; in section 3 we analyze the data in detail as a function of frequency; section 4 is devoted to interpretation of the observed propagation mode; in section 5 we show results of a ray-tracing simulation based on the measurements; in section 6 we interpret and discuss our results.

## 2. Observations of Equatorial Noise at Low Altitudes

The DEMETER spacecraft operated from 2004 to 2010 on a circular nearly Sun-synchronous orbit at an altitude of approximately 700 km. We analyze six-component measurements of the electric and magnetic fields [Parrot *et al.*, 2006; Berthelier *et al.*, 2006a; Santolík *et al.*, 2006] recorded during the burst-mode intervals as 16-bit waveforms with a sampling frequency of 2.5 kHz. From their power-frequency spectrograms we have identified 47 events with a clear structure of spectral lines within 20° from the geomagnetic equator, systematically excluding cases of power-line harmonic radiation [Němec *et al.*, 2007]. The selected events mostly occur during high geomagnetic activity, with the main occurrence peak within  $\pm 10^\circ$  of geomagnetic latitude. All of them show similar characteristics which might be consistent with properties of equatorial noise. Five of these events have been briefly reported by Němec *et al.* [2007], but no analysis of propagation, wave mode, and spectral properties has been done. Here we analyze in detail another case of this set which has been selected for its particularly clear wave polarization properties.

The selected observations have been recorded on 12 April 2005 between 03:27 and 03:40 UT when the spacecraft moved above the Pacific coast of South America to the Gulf of Mexico during a nightside orbit with a nearly constant magnetic local time from 22:30 to 21:50 at an altitude from 709 to 705 km. The geomagnetic  $K_p$  index reached 5, and the  $AE$  index increased over 800 nT in the main phase of a moderate geomagnetic storm with the minimum  $Dst$  index below  $-60$  nT, following a previous increase of the solar wind density up to  $50 \text{ cm}^{-3}$  and a subsequent pronounced southward turning of the interplanetary magnetic field.

Figures 1a and 1b, respectively, show frequency-time spectrograms of the total power of the electric and magnetic fields, with a frequency resolution of 3.7 Hz. A structure of strong electromagnetic spectral lines is well seen in the first part of the time interval before 03:33 UT at frequencies of 150–250 Hz, with a low-intensity emission spanning up to 400 Hz. These waves, as we are going to show, can be attributed to equatorial noise, unlike the bursts of electromagnetic waves caused by lightning-generated whistlers and occurring after 03:33 UT. Propagation of this type of waves has been analyzed in detail from the DEMETER data previously [Santolík *et al.*, 2008, 2009; Shklyar *et al.*, 2012]. In our case the bursts are generally limited below the local proton cyclotron frequency ( $f_{H^+}$ , shown by a black solid line), with some of them reaching above that limit, especially toward the end of the analyzed time interval.

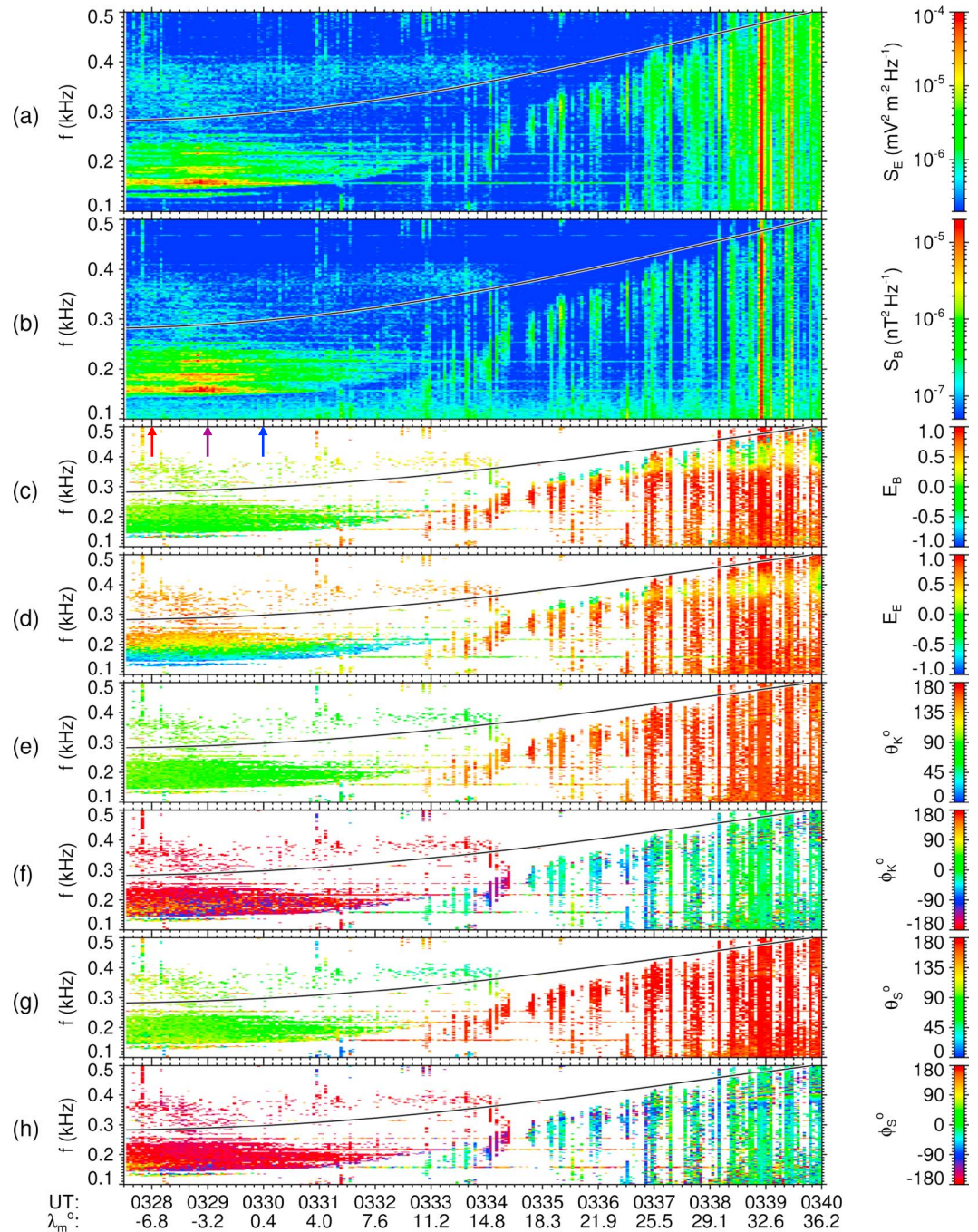


**Figure 1.** Example of the burst-mode observations of the DEMETER spacecraft on 12 April 2005. Frequency-time plots of (a) the sum of the power-spectral densities of three orthogonal electric field components, (b) the sum of the power-spectral densities of three orthogonal magnetic field components, (c) the ellipticity of the magnetic field polarization with a sign corresponding to the sense of polarization, (d) the ellipticity of the electric field polarization with a sign corresponding to the sense of polarization, (e) the angle between the wave vector and the background magnetic field, (f) azimuth of the wave vector with respect to the outward direction, positive eastward, (g) the angle between the Poynting vector and the background magnetic field, and (h) azimuth of the Poynting vector with respect to the outward direction. A color scale is given on the right-hand side of each plot. Values in Figures 1c–1h are plotted only for electric and magnetic power-spectral densities above  $10^{-7} \text{ nT}^2 \text{ Hz}^{-1}$  and  $5 \times 10^{-7} \text{ mV}^2 \text{ m}^{-2} \text{ Hz}^{-1}$ , respectively. Arrows point to the three time intervals selected for Figure 2. The local proton cyclotron frequency is given by a black solid line in each plot. Time is given in UT on the bottom, as well as the geomagnetic latitude of the spacecraft.

With the full 3-D measurement of the magnetic field fluctuations we have used the singular value decomposition (SVD) method [Santolik *et al.*, 2002b] to calculate the ellipticity of magnetic polarization shown in Figure 1c. Values close to zero correspond to linear polarization, while  $-1$  and  $+1$  mean left- or right-handed circular polarization, respectively. While the magnetic field polarization is linear before 03:33 UT, the same analysis of the electric field polarization (Figure 1d) gives progressively increasing values from left-hand circular through linear to right-hand circular polarization, as a function of increasing frequency. After 03:33 UT, both the magnetic and electric field polarization show another pattern: right-hand circular polarization at low frequencies, with an excursion to linear and left-handed polarization, and then return back to the right-hand circular polarization at higher frequencies.

The full 6-D measurements of the magnetic and electric field fluctuations also allow us to determine the wave vector direction using the SVD method [Santolik *et al.*, 2003]. The results, shown in Figures 1e and 1f, indicate perpendicular and downward propagating waves before 03:33 UT, and after that time we detect mainly upward waves propagating nearly antiparallel to the geomagnetic field, i.e., toward the equator. Very similar pattern is obtained from an independent analysis of the direction of the Poynting vector [Santolik *et al.*, 2001] shown in Figures 1g and 1h.

### 3. Detailed Spectral Analysis of Equatorial Noise

The red, purple, and blue arrows in Figure 1c, respectively, point to three 10 s intervals around 03:28, 03:29, and 03:30 UT. These intervals are analyzed in detail in Figure 2, using the same color coding for line plots as a function of frequency with a resolution of 1.2 Hz. In agreement with original observations of Gurnett [1976] we see a complex superposition of many harmonically spaced lines with different frequency spacings in Figures 2a and 2b. For example, black arrows show the 18th, 19th, 22nd, and 23rd harmonics of 9.9 Hz, which correspond to a hypothetical source of proton cyclotron harmonics located at an approximate radial distance of  $3.6 R_E$ . Grey arrows show the 42nd-51st harmonics of 3.69 Hz, corresponding to  $f_{H^+}$  at  $5.1 R_E$ . Alternatively, we may also interpret them as harmonics of  $He^+$  or  $O^+$  cyclotron frequencies ( $f_{He^+}$  or  $f_{O^+}$ ) at  $3.2$  or  $2.0 R_E$ , respectively. This structure is similar in both electric and magnetic field spectra and in all three time intervals, while the local  $f_{H^+}$  is changing from 284 to 297 Hz (see Figure 2a), suggesting again a distant source. However, the electric field spectra in Figure 2a also show a line varying in frequency from 131 to 137 Hz and following thus the variation of the local  $f_{H^+}$  at approximately 46% of its value. This line is nearly absent in the magnetic field spectra in Figure 2b. The local origin in the ion Bernstein mode is probable either close to the second harmonic of local  $f_{He^+}$  or close to the eighth harmonic of local  $f_{O^+}$ . Hypothetically, it could be also close to the fundamental cyclotron frequency of deuterium ions or  $He^{2+}$ .

The electric field spectra show a sharp lower cutoff which also varies with the local  $f_{H^+}$ , being at 127 Hz in the most intense part of the emission around 03:29 UT (purple line). The magnetic field ellipticity (Figure 2c) always gives linear polarization for the intense part of the emission as well as for the weaker waves up to 400 Hz, with exceptions of very narrow frequency bands around higher harmonics of 19.52 Hz, caused by artificial interferences linked to the onboard digital processing (marked by vertical dotted lines). The electric field ellipticity (Figure 2d) consistently shows a pattern of changing polarization from left-hand circular to right-hand circular. The change of the sense of polarization happens approximately at 183 Hz in the interval around 03:29 UT (purple line). The wave vector and Poynting vector directions in Figures 2e–2h independently show the propagation properties in a much more detailed way than in the color spectrograms in Figure 1. The waves propagate toward the Earth, very close to the plane of the magnetic meridian, at angles close to perpendicular to the local geomagnetic field line. A slightly southward inclination of the Poynting vector can be identified in Figure 2g for the interval around 03:28 UT (red line), which was recorded to the south from the equator. A remarkably similar propagation pattern is also observed for the weaker waves up to 400 Hz.

### 4. Interpretation of the Observed Polarization Properties

The observed line structure and propagation properties strongly suggest that the waves recorded before 03:33 UT are formed as equatorial noise and propagate down to the low orbiting spacecraft from different distant sources. The main difference from typical equatorial noise is the sharp lower cutoff, which moves up in frequency as the local  $f_{H^+}$  increases along the orbit (Figure 1a), as well as changes in the polarization

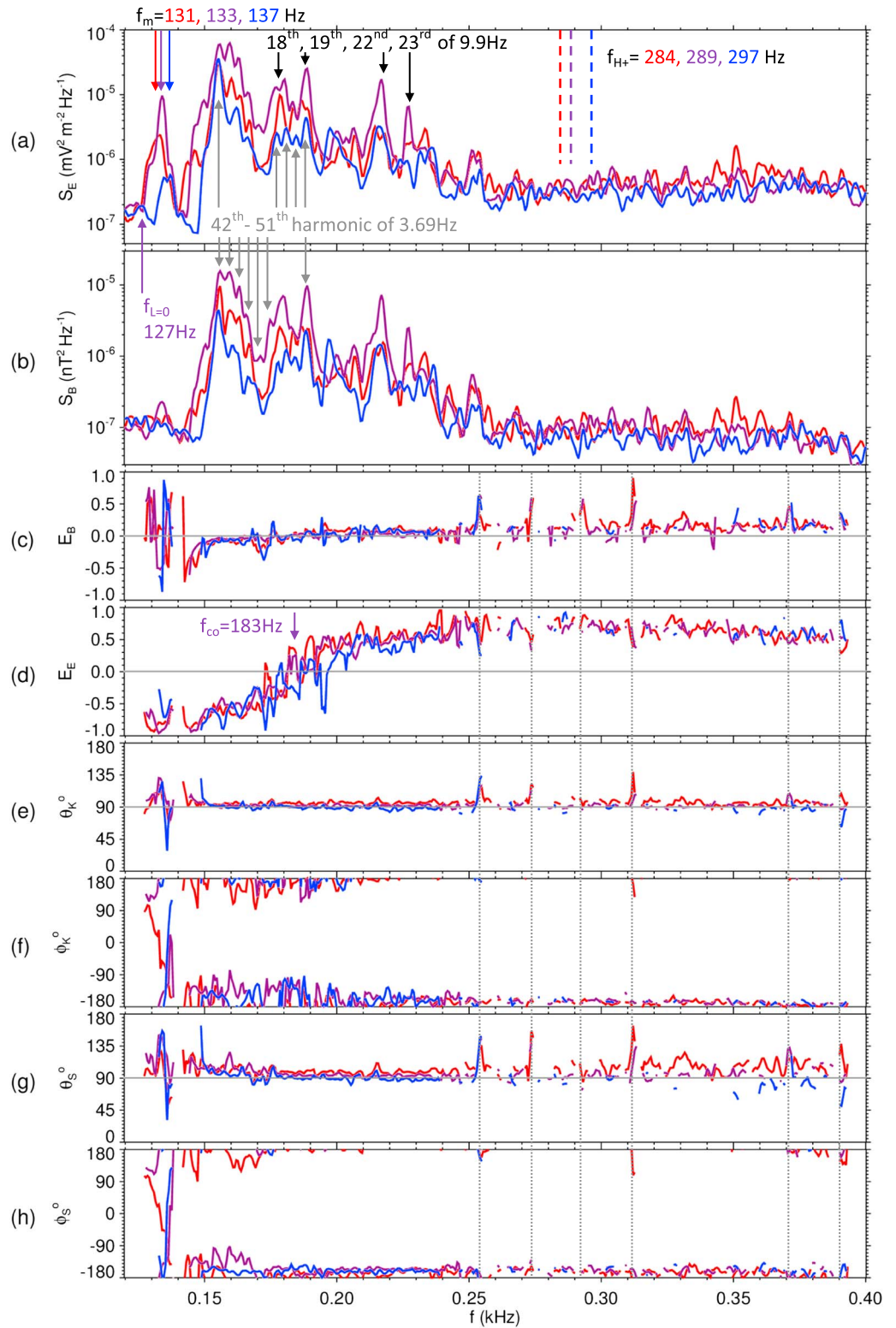


**Figure 2.** Detailed analysis of 10 s time intervals marked by arrows in Figure 1c. Blue, magenta, and red lines show the results for intervals centered at 13:28 UT, 13:29 UT, and 13:30 UT, respectively. (a–h) The description of separate panels is the same as in Figure 1. Arrows show the characteristic frequencies for the three time intervals and identified harmonics in the observed line structure. Vertical dotted lines denote instrumental interferences.

sense of the electric field (Figure 1d). The sharp cutoff can correspond to  $L = 0$  cutoff occurring below  $f_{H^+}$  [Stix, 1992] for downward propagating waves [Gurnett and Burns, 1968; Santolík and Parrot, 1999],

$$f_{L=0} = f_{H^+} \frac{1 + P_O(R_{OH} - 1)}{R_{OH}} \quad (1)$$

where  $R_{OH} = 16$  is the ratio of masses of oxygen to hydrogen ions assuming a two-component plasma. With the observed values at 03:29 UT ( $f_{L=0} = 127$  Hz,  $f_{H^+} = 289$  Hz), this equation gives the relative  $O^+$  fraction  $P_O = 40.2\%$ . Between  $f_{L=0}$  and  $f_{H^+}$  the theory also predicts a crossover frequency of polarization reversal,

$$f_{co} = f_{H^+} \frac{\sqrt{1 + P_O(R_{OH}^2 - 1)}}{R_{OH}} \quad (2)$$

With the observed  $f_{co} = 183$  Hz we obtain  $P_O = 39.9\%$ , in a remarkable agreement with the results from equation (1).

The downward propagating equatorial noise observed in Figure 1 before 03:33 UT can be therefore attributed to the theoretical cold plasma mode shown in Figure 3a, at frequencies above the lower cutoff at  $f_{L=0}$ . This mode is coupled by a smooth variation of the refractive index to the whistler mode, so it is appropriate to refer to equatorial noise as the whistler mode waves. Oppositely, Figure 3b shows the second possible theoretical cold plasma mode at the frequencies below  $f_{H^+}$ . It corresponds to the proton cyclotron branch, and, at frequencies well below  $f_{O^+}$ , it is coupled to the low-frequency magnetosonic mode, also known as compressional Alfvén waves. Unless the wave vector is at zero angle  $\theta_K$  to the background magnetic field, there is a sharp discontinuity of refractive indices of the whistler mode in Figure 3a and the magnetosonic-proton cyclotron mode in Figure 3b. There is therefore no possibility to connect equatorial noise to the low-frequency magnetosonic mode by a smooth variation of the refractive index in a plasma with multiple ions.

Our observations show that equatorial noise propagates downward with nearly perpendicular  $\theta_K$  (Figure 2e). The theory (Figure 3c) shows that the Poynting vector angle  $\theta_S$  should also be perpendicular. This is in agreement with the observations in Figure 2g. However, when  $\theta_K$  deviates from the perpendicular direction, we obtain a difference in the directions of the wave vector and of the Poynting vector (Figure 3c), especially at higher frequencies.

The theory (Figure 3e) well reproduces the observed linear polarization of magnetic field fluctuations (Figure 2c). Polarization of the electric field varies with increasing frequency from left-hand circular to right-hand circular, with a smooth polarization reversal at  $f_{co}$  (Figure 3g), in agreement with our observations in Figure 2d. Approaching  $f_{L=0}$  from above the power of magnetic field fluctuations of this mode becomes weaker relative to the electric field power (Figure 3i). The theory gives a factor of nearly 5 between waves at frequencies of 155 Hz and 133 Hz. This may in part explain the absence of the peak just above  $f_{L=0}$  in Figure 2b, where the magnetic field power changes between these frequencies by 1 order of magnitude more than the electric field power in Figure 2a.

As a validation of our analysis, the lightning-generated waves recorded after 03:33 UT also show properties consistent with the theory. During their outward but mainly antiparallel propagation with respect the geomagnetic field (equivalent to small  $\theta_K$  angles for the mode in Figure 3b, both below and above the multiion hybrid frequency  $f_{ih}$  at 60 Hz), a part of their power departs into the left-hand polarized (Figures 3f and 3h) proton cyclotron whistlers [Gurnett *et al.*, 1965] with a resonance at  $f_{H^+}$ , but another part occurs in the right-hand polarized whistler mode, which continues above  $f_{H^+}$  as it is seen at small  $\theta_K$  angles in Figures 3e and 3g.

## 5. Ray-Tracing Simulation

Ray-tracing simulations of equatorial noise have been performed in the past, for example, by Kasahara *et al.* [1994], Boardsen *et al.* [1992, 2016], and Xiao *et al.* [2012], but the results did not show the possibility of inward propagating waves, which was nevertheless indicated by a simplified theoretical analysis of Chen and Thorne [2012]. Walker *et al.* [2015b] recently simulated outward radial propagation from a distance of  $3.5 R_E$ . Figure 4 presents the first results of inward ray tracing of equatorial noise, showing the possibility that equatorial noise reaches the low-Earth orbit where we observe it. We use a dipole model of the geomagnetic field and a diffusive equilibrium plasma model with boundary conditions corresponding to measurements on board

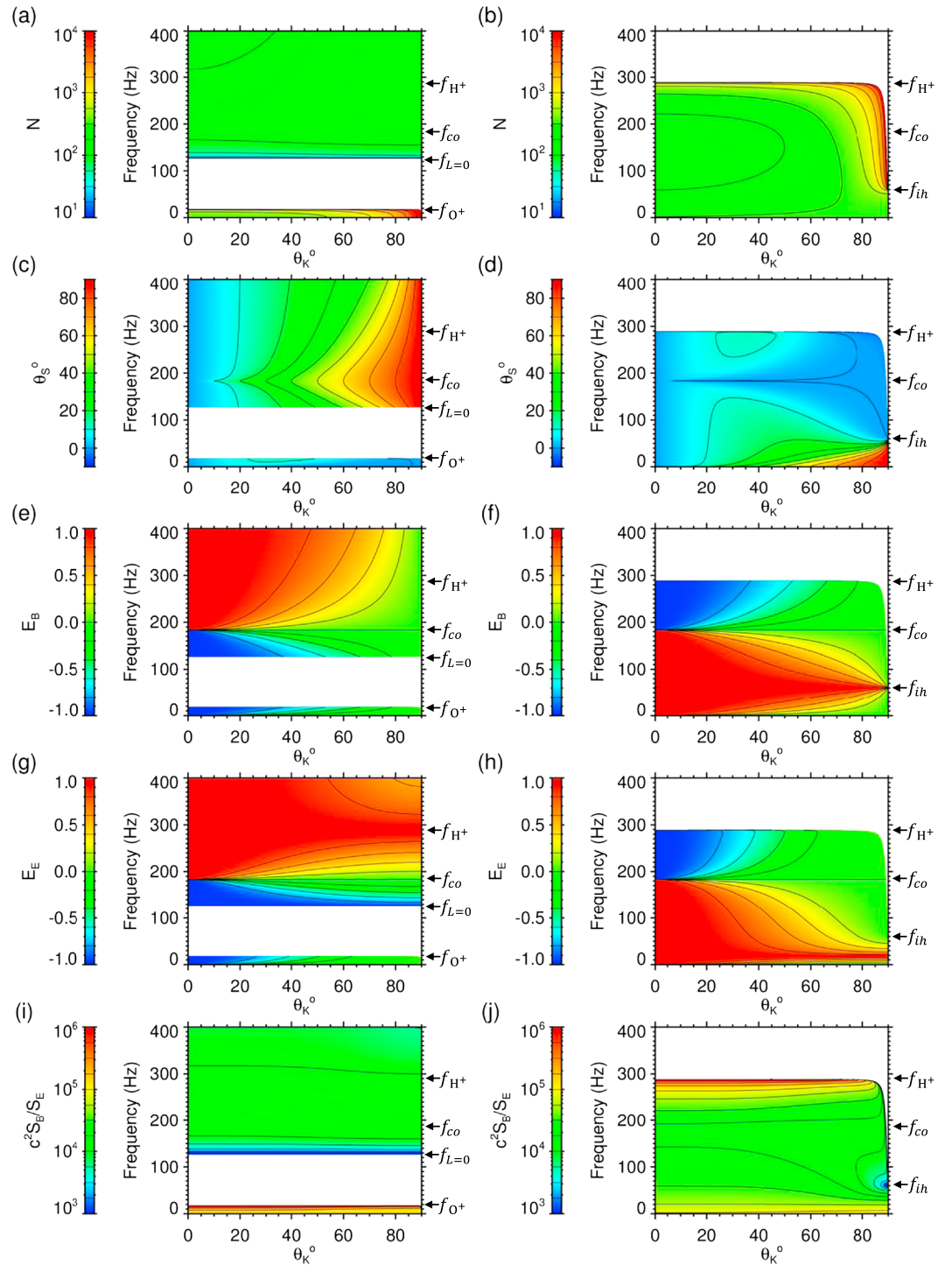


**Figure 3.** Theoretical properties of cold plasma wave modes below 400 Hz as a function of frequency and angle  $\theta_K$  between the wave vector and the background magnetic field. We assume a three-component plasma model with parameters derived from observations at 03:29 UT (purple line in Figure 2): 60%  $H^+$  ions, 40%  $O^+$  ions, and electrons with a plasma density of  $3 \times 10^4 \text{ cm}^{-3}$ . Geomagnetic field strength corresponds to  $f_{H^+} = 289 \text{ Hz}$ . Results are symmetric for  $\theta_K$  and  $180^\circ - \theta_K$ . Properties of the shear Alfvén-oxygen cyclotron mode (below  $f_{O^+}$ ) and of the whistler mode (above  $f_{L=0}$ ) are given on the left-hand side. Magnetosonic-proton cyclotron mode (below  $f_{H^+}$ ) is shown on the right-hand side. (a and b) Refractive index, (c and d) angle between the Poynting vector and the background magnetic field, (e and f) ellipticity of the magnetic field polarization with a sign corresponding to the sense of polarization, (g and h) ellipticity of the electric field polarization with a sign corresponding to the sense of polarization, and (i and j) dimensionless ratio of magnetic to electric power. Black lines represent the isocontours shown on the color scales for each figure.

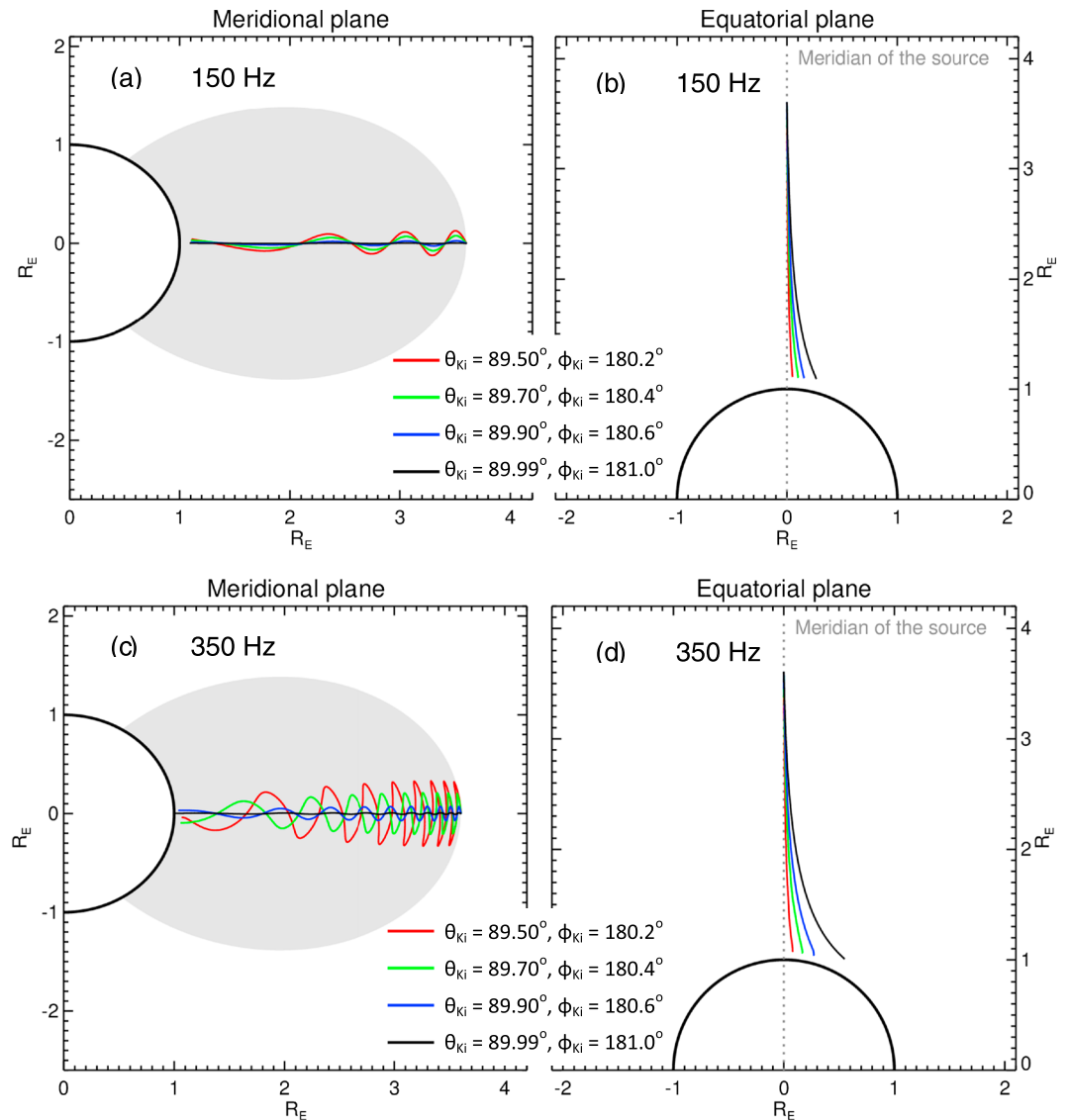


**Figure 4.** Results of a 3-D ray-tracing simulation with four color-coded initial wave vector directions (defined by angles  $\theta_{Ki}$  and  $\varphi_{Ki}$ ) in the source at  $3.6 R_E$  (a) for a wave frequency of 150 Hz, projected onto the plane of the local magnetic meridian; area inside the dipole field line which crosses the equator at a radial distance of  $3.6 R_E$  is greyed; (b) for 150 Hz, projected on the magnetic equatorial plane, dotted line shows the local magnetic meridian of the source; (c) for 350 Hz, projected onto the plane of the local magnetic meridian; and (d) for 350 Hz, projected on the magnetic equatorial plane.

DEMETER. For an altitude of 708 km we use the same three-component plasma model as in Figure 3: the ion composition of 60%  $H^+$  and 40%  $O^+$  has been derived from our observations of characteristic frequencies  $f_{L=0}$  and  $f_{co}$ ; plasma density of  $3 \times 10^4 \text{ cm}^{-3}$  and temperature of 1000 K correspond to measurements of the IAP ion analyzer [Berthelier et al., 2006b]. This temperature defines the radial density profiles of the two ions with a rapidly decreasing fraction of  $O^+$ . It reaches 99% at an altitude of 380 km below the spacecraft, it falls down below 1% at 1000 km and below 0.1% at 1200 km.

The calculations have been done by a 3-D ray-tracing code with verification of the Wentzel-Kramers-Brillouin approximation of geometric optics in every integration step, as it is described by Santolík et al. [2009]. Wave propagation is simulated for the previously identified propagation mode (whistler mode from Figure 3a) at a peak frequency of 150 Hz and also at a frequency of 350 Hz in the weak part of the observed equatorial noise emission. The waves are launched from a radial distance of  $3.6 R_E$  corresponding to one of the observed systems of spectral lines which are shown by black arrows in Figure 2. Results in Figures 4a

and 4c exhibit oscillations of the rays around the equatorial plane. These oscillations increase their amplitude with frequency, as does the difference between the directions of the wave vector and of the Poynting vector (see Figure 3c). They also grow if the initial wave vectors are more deviated from the perpendicular direction. However, the inward propagation seems to focus the waves more toward the equator, as the amplitude of oscillations decreases when the waves propagate toward the Earth, reaching eventually the DEMETER orbit. This can, however, happen only if the initial wave vectors are very close to the plane of the local magnetic meridian, as it is shown in Figures 4b and 4d. Outside this plane, propagation toward the Earth causes a strong change of the wave vector azimuth which, in turn, bends the ray more and more away from the meridional plane. An initial deviation by more than  $1^\circ$  is sufficient to deflect the simulated ray above the DEMETER altitude at 350 Hz in Figure 4d. This effect is less pronounced at 150 Hz enabling thus waves at lower frequencies to better penetrate down to low altitudes.

## 6. Discussion

The ray-tracing analysis shows that propagation of equatorial noise down to an altitude of 700 km is possible if the wave frequency stays above the local  $L = 0$  cutoff. This is more likely to happen if the waves are generated within the plasmasphere where their frequencies are generally higher [Němec *et al.*, 2015a; Boardson *et al.*, 2016]. However, further penetration of equatorial noise down to the ground is excluded, at least for the analyzed event: the downward propagating wave would encounter an increasing geomagnetic field and hence increasing  $f_{H^+}$ . Additionally, the  $O^+$  fraction would also increase, causing that the  $L = 0$  cutoff frequency becomes closer to  $f_{H^+}$  according to equation (1). Altogether this would in our case mean that the  $L = 0$  cutoff would shift up to approximately 380 Hz at an altitude of 100 km, effectively wiping out the entire observed frequency range of equatorial noise and preventing it from penetrating into the Earth-ionosphere waveguide. In any case, it is rare for equatorial noise to reach frequencies above 400 Hz with higher intensities [Němec *et al.*, 2015a; Boardson *et al.*, 2016]; therefore, the possibility of further penetration to the ground seems to be unlikely in general.

The penetration to the ground becomes even less probable if we consider the progressive azimuthal bending of the rays approaching the Earth, as it is shown in Figures 4b and 4d. The condition of nearly radial wave vectors in the source, however, appears already very restrictive for allowing waves to propagate down to an altitude of 700 km, where we experimentally detect them. For one of the anticipated sources whose location at a radial distance at  $3.6 R_E$  is based on a part of the harmonic line structure identified in measured frequency spectra, we need to generate the waves within  $1^\circ$  from the radial direction at a frequency of 350 Hz. It seems very unlikely that the source would radiate in such a limited azimuthal range, as the resonant condition does not generally depend on azimuthal angle. A probable explanation is that we only see a small fraction of generated waves which propagate nearly radially while most of them propagate elsewhere.

Our observation of weaker equatorial noise at frequencies above 250 Hz in Figures 1a and 1b might be related to the fact that the ray-bending effect becomes more pronounced, and therefore, the interval of possible azimuths is more restricted at higher frequencies. This probably overweighs the effect discussed by Chen *et al.* [2016], who concluded that equatorial noise with a continuous spectrum, as we observe it above 250 Hz, should be more intense than equatorial noise with pronounced spectral lines. Geomagnetically disturbed conditions cause equatorial noise to generally increase its occurrence and intensity at all frequencies [e.g., Hrbáčková *et al.*, 2015; Němec *et al.*, 2015a], favoring therefore penetration of detectable wave power to low altitudes.

Future systematic analysis of this phenomenon is necessary in order to draw firm conclusions on the geophysical conditions under which equatorial noise penetrates to low altitudes. Further study is also needed concerning the possibility of quasiperiodic modulation in these cases.

## References

- Balikhin, M. A., Y. Y. Shprits, S. N. Walker, L. Chen, N. Cornilleau-Wehrlin, I. Dandouras, O. Santolik, C. Carr, K. H. Yearby, and B. Weiss (2015), Observations of discrete harmonics emerging from equatorial noise, *Nat. Commun.*, *6*, 7703, doi:10.1038/ncomms8703.
- Berthelier, J. J., et al. (2006a), ICE, the electric field experiment on DEMETER, *Planet. Space Sci.*, *54*, 456–471.
- Berthelier, J., M. Godefroy, F. Leblanc, E. Seran, D. Peschard, P. Gilbert, and J. Artru (2006b), IAP, the thermal plasma analyzer on DEMETER, *Planet. Space Sci.*, *54*, 487–501.

### Acknowledgments

DEMETER was a CNES mission. We thank the engineers from CNES and scientific laboratories (CBK, IRAP, LPC2E, LPP, and SSD of ESTEC) who largely contributed to the success of this mission. DEMETER data are accessible from <http://cdpp2.cnes.fr/cdpp>. This work was supported by GACR grants 14-31899S and 15-01775Y, MSMT grant LH 15304, and by the Praemium Academiae award from the CAS.

- Boardsen, S. A., D. L. Gallagher, D. A. Gurnett, W. K. Peterson, and J. L. Green (1992), Funnel-shaped, low-frequency equatorial waves, *J. Geophys. Res.*, *97*, 14,967–14,976, doi:10.1029/92JA00827.
- Boardsen, S. A., G. B. Hospodarsky, C. A. Kletzing, R. F. Pfaff, W. S. Kurth, J. R. Wygant, and E. A. MacDonald (2014), Van Allen Probe observations of periodic rising frequencies of the fast magnetosonic mode, *Geophys. Res. Lett.*, *41*, 8161–8168, doi:10.1002/2014GL062020.
- Boardsen, S. A., et al. (2016), Survey of the frequency dependent latitudinal distribution of the fast magnetosonic wave mode from Van Allen Probes Electric and Magnetic Field Instrument and Integrated Science waveform receiver plasma wave analysis, *J. Geophys. Res. Space Physics*, *121*, 2902–2921, doi:10.1002/2015JA021844.
- Bortnik, J., R. M. Thorne, B. Ni, and J. Li (2015), Analytical approximation of transit time scattering due to magnetosonic waves, *Geophys. Res. Lett.*, *42*, 1318–1325, doi:10.1002/2014GL062710.
- Chen, L., and R. M. Thorne (2012), Perpendicular propagation of magnetosonic waves, *Geophys. Res. Lett.*, *39*, L14102, doi:10.1029/2012GL052485.
- Chen, L., J. Sun, Q. Lu, X. Gao, Z. Xia, and Z. Zhima (2016), Generation of magnetosonic waves over a continuous spectrum, *J. Geophys. Res. Space Physics*, *121*, 1137–1147, doi:10.1002/2015JA022089.
- Fu, H. S., J. B. Cao, Z. Zhima, Y. V. Khotyaintsev, V. Angelopoulos, O. Santolík, Y. Omura, U. Taubenschuss, L. Chen, and S. Y. Huang (2014), First observation of rising-tone magnetosonic waves, *Geophys. Res. Lett.*, *41*, 7419–7426, doi:10.1002/2014GL061867.
- Gurnett, D. A. (1976), Plasma wave interactions with energetic ions near the magnetic equator, *J. Geophys. Res.*, *81*, 2765–2770, doi:10.1029/JA081i016p02765.
- Gurnett, D. A., and T. B. Burns (1968), The low-frequency cutoff of ELF emissions, *J. Geophys. Res.*, *73*, 7437–7445, doi:10.1029/JA073i023p07437.
- Gurnett, D. A., S. D. Shawhan, N. M. Brice, and R. L. Smith (1965), Ion cyclotron whistlers, *J. Geophys. Res.*, *70*, 1665–1688, doi:10.1029/JZ070i007p01665.
- Horne, R. B., G. V. Wheeler, and H. S. C. K. Alleyne (2000), Proton and electron heating by radially propagating fast magnetosonic waves, *J. Geophys. Res.*, *105*, 27,597–27,610, doi:10.1029/2000JA000018.
- Horne, R. B., R. M. Thorne, S. A. Glauert, N. P. Meredith, D. Pokhotelov, and O. Santolík (2007), Electron acceleration in the Van Allen radiation belts by fast magnetosonic waves, *Geophys. Res. Lett.*, *34*, L17107, doi:10.1029/2007GL030267.
- Hrbáčková, Z., O. Santolík, F. Němec, E. Macúšová, and N. Cornilleau-Wehrin (2015), Systematic analysis of occurrence of equatorial noise emissions using 10 years of data from the Cluster mission, *J. Geophys. Res. Space Physics*, *120*, 1007–1021, doi:10.1002/2014JA020268.
- Kasahara, Y., H. Kenmochi, and I. Kimura (1994), Propagation characteristics of the ELF emissions observed by the satellite Akebono in the magnetic equatorial region, *Radio Sci.*, *29*, 751–767, doi:10.1029/94RS00445.
- Laakso, H., H. Junginger, A. Roux, R. Schmidt, and C. de Villedary (1990), Magnetosonic waves above  $f_{CH^+}$  at geostationary orbit: GEOS 2 results, *J. Geophys. Res.*, *95*, 10,609–10,621, doi:10.1002/2016GL069582.
- Li, J., B. Ni, L. Xie, Z. Pu, J. Bortnik, R. M. Thorne, and L. Chen (2014), Interactions between magnetosonic waves and radiation belt electrons: Comparisons of quasi-linear calculations with test particle simulations, *Geophys. Res. Lett.*, *41*, 4828–4834, doi:10.1002/2014GL060461.
- Ma, Q., W. Li, R. M. Thorne, and V. Angelopoulos (2013), Global distribution of equatorial magnetosonic waves observed by THEMIS, *Geophys. Res. Lett.*, *40*, 1895–1901, doi:10.1002/grl.50434.
- Ma, Q., W. Li, L. Chen, R. M. Thorne, and V. Angelopoulos (2014), Magnetosonic wave excitation by ion ring distributions in the Earth's inner magnetosphere, *J. Geophys. Res. Space Physics*, *119*, 844–852, doi:10.1002/2013JA019591.
- Ma, Q., W. Li, R. M. Thorne, J. Bortnik, C. A. Kletzing, W. S. Kurth, and G. B. Hospodarsky (2016), Electron scattering by magnetosonic waves in the inner magnetosphere, *J. Geophys. Res. Space Physics*, *121*, 274–285, doi:10.1002/2015JA021992.
- Meredith, N. P., R. B. Horne, and R. R. Anderson (2008), Survey of magnetosonic waves and proton ring distributions in the Earth's inner magnetosphere, *J. Geophys. Res.*, *113*, A06213, doi:10.1029/2007JA012975.
- Min, K., and K. Liu (2016), Understanding the growth rate patterns of ion Bernstein instabilities driven by ring-like proton velocity distributions, *J. Geophys. Res. Space Physics*, *121*, 3036–3049, doi:10.1002/2016JA022524.
- Němec, F., O. Santolík, K. Gereova, E. Macusova, Y. de Conchy, and N. Cornilleau-Wehrin (2005), Initial results of a survey of equatorial noise emissions observed by the Cluster spacecraft, *Planet. Space Sci.*, *53*, 291–298.
- Němec, F., O. Santolík, K. Gereova, E. Macusova, H. Laakso, Y. de Conchy, M. Maksimovic, and N. Cornilleau-Wehrin (2006), Equatorial noise: Statistical study of its localization and the derived number density, *Adv. Space Res.*, *37*, 610–616.
- Němec, F., O. Santolík, M. Parrot, and J. J. Berthelier (2007), Comparison of magnetospheric line radiation and power line harmonic radiation: A systematic survey using the DEMETER spacecraft, *J. Geophys. Res.*, *112*, A04301, doi:10.1029/2006JA012134.
- Němec, F., O. Santolík, J. S. Pickett, Z. Hrbáčková, and N. Cornilleau-Wehrin (2013), Azimuthal directions of equatorial noise propagation determined using 10 years of data from the Cluster spacecraft, *J. Geophys. Res. Space Physics*, *118*, 7160–7169, doi:10.1002/2013JA019373.
- Němec, F., O. Santolík, Z. Hrbáčková, and N. Cornilleau-Wehrin (2015a), Intensities and spatiotemporal variability of equatorial noise emissions observed by the Cluster spacecraft, *J. Geophys. Res. Space Physics*, *120*, 1620–1632, doi:10.1002/2014JA020814.
- Němec, F., O. Santolík, Z. Hrbáčková, J. S. Pickett, and N. Cornilleau-Wehrin (2015b), Equatorial noise emissions with quasiperiodic modulation of wave intensity, *J. Geophys. Res. Space Physics*, *120*, 2649–2661, doi:10.1002/2014JA020816.
- Parrot, M., et al. (2006), The magnetic field experiment IMSC and its data processing onboard DEMETER: Scientific objectives, description and first results, *Planet. Space Sci.*, *54*, 441–455.
- Perraut, S., A. Roux, P. Robert, R. Gendrin, J. A. Sauvaud, J. M. Bosqued, G. Kremser, and A. Korth (1982), A systematic study of ULF waves above  $FH^+$  from GEOS 1 and 2 measurements and their relationships with proton ring distributions, *J. Geophys. Res.*, *87*, 6219–6236, doi:10.1029/JA087iA08p06219.
- Posch, J. L., M. J. Engebretson, C. N. Olson, S. A. Thaller, A. W. Breneman, J. R. Wygant, S. A. Boardsen, C. A. Kletzing, C. W. Smith, and G. D. Reeves (2015), Low-harmonic magnetosonic waves observed by the Van Allen Probes, *J. Geophys. Res. Space Physics*, *120*, 6230–6257, doi:10.1002/2015JA021179.
- Russell, C. T., R. E. Holzer, and E. J. Smith (1970), OGO 3 observations of ELF noise in the magnetosphere. The nature of equatorial noise, *J. Geophys. Res.*, *75*, 755–768, doi:10.1029/JA075i004p00755.
- Santolík, O., and M. Parrot (1999), Case studies on wave propagation and polarization of ELF emissions observed by Freja around the local proton gyro-frequency, *J. Geophys. Res.*, *104*(A2), 2459–2475, doi:10.1029/1998JA900045.
- Santolík, O., F. Lefevre, M. Parrot, and J. L. Rauch (2001), Complete wave-vector directions of electromagnetic emissions: Application to INTERBALL-2 measurements in the nightside auroral zone, *J. Geophys. Res.*, *106*, 13,191–13,201, doi:10.1029/2000JA000275.
- Santolík, O., J. S. Pickett, D. A. Gurnett, M. Maksimovic, and N. Cornilleau-Wehrin (2002a), Spatiotemporal variability and propagation of equatorial noise observed by Cluster, *J. Geophys. Res.*, *107*(A12), 1495, doi:10.1029/2001JA009159.
- Santolík, O., J. S. Pickett, D. A. Gurnett, and L. R. O. Storey (2002b), Magnetic component of narrow-band ion cyclotron waves in the auroral zone, *J. Geophys. Res.*, *107*(A12), 1444, doi:10.1029/2001JA000146.

- Santolík, O., M. Parrot, and F. Lefeuvre (2003), Singular value decomposition methods for wave propagation analysis, *Radio Sci.*, *38*(1), 1010, doi:10.1029/2000RS002523.
- Santolík, O., F. Němec, K. Gereová, E. Macúšová, Y. de Conchy, and N. Cornilleau-Wehrin (2004), Systematic analysis of equatorial noise below the lower hybrid frequency, *Ann. Geophys.*, *22*, 2587–2595.
- Santolík, O., F. Němec, M. Parrot, D. Lagoutte, L. Madrias, and J. J. Berthelier (2006), Analysis methods for multi-component wave measurements on board the DEMETER spacecraft, *Planet. Space Sci.*, *54*, 512–527.
- Santolík, O., M. Parrot, and J. Chum (2008), Propagation spectrograms of whistler-mode radiation from lightning, *IEEE Trans. Plasma Sci.*, *36*(4), 1166–1167, doi:10.1109/TPS.2008.920899.
- Santolík, O., M. Parrot, U. S. Inan, D. Buresova, D. A. Gurnett, and J. Chum (2009), Propagation of unducted whistlers from their source lightning: A case study, *J. Geophys. Res.*, *114*, A03212, doi:10.1029/2008JA013776.
- Shklyar, D. R., L. R. O. Storey, J. Chum, F. Jiricek, F. Nemeč, M. Parrot, O. Santolík, and E. E. Titova (2012), Spectral features of lightning-induced ion cyclotron waves at low latitudes: DEMETER observations and simulation, *J. Geophys. Res.*, *117*, A12206, doi:10.1029/2012JA018016.
- Shprits, Y. Y. (2016), Estimation of bounce resonant scattering by fast magnetosonic waves, *Geophys. Res. Lett.*, *43*, 998–1006, doi:10.1002/2015GL066796.
- Stix, T. H. (1992), *Waves in Plasmas*, Springer, New York.
- Tsurutani, B., B. J. Falkowski, J. S. Pickett, O. P. Verkhoglyadova, O. Santolík, and G. S. Lakhina (2014), Extremely intense ELF magnetosonic waves: A survey of polar observations, *J. Geophys. Res. Space Physics*, *119*, 964–977, doi:10.1002/2013JA019284.
- Walker, S. N., M. A. Balikhin, P. Canu, N. Cornilleau-Wehrin, and I. Moiseenko (2015a), Investigation of the Chirikov resonance overlap criteria for equatorial magnetosonic waves, *J. Geophys. Res. Space Physics*, *120*, 8774–8781, doi:10.1002/2015JA021718.
- Walker, S. N., M. A. Balikhin, D. R. Shklyar, K. H. Yearby, P. Canu, C. M. Carr, and I. Dandouras (2015b), Experimental determination of the dispersion relation of magnetosonic waves, *J. Geophys. Res. Space Physics*, *120*, 9632–9650, doi:10.1002/2015JA021746.
- Xiao, F., Q. Zhou, Z. He, and L. Tang (2012), Three-dimensional ray tracing of fast magnetosonic waves, *J. Geophys. Res.*, *117*, A06208, doi:10.1029/2012JA017589.
- Xiao, F., Q. Zhou, Y. He, C. Yang, S. Liu, D. N. Baker, H. E. Spence, G. D. Reeves, H. O. Funsten, and J. B. Blake (2015), Penetration of magnetosonic waves into the plasmasphere observed by the Van Allen Probes, *Geophys. Res. Lett.*, *42*, 7287–7294, doi:10.1002/2015GL065745.
- Zhima, Z., L. Chen, H. Fu, J. Cao, R. B. Horne, and G. Reeves (2015), Observations of discrete magnetosonic waves off the magnetic equator, *Geophys. Res. Lett.*, *42*, 9694–9701, doi:10.1002/2015GL066255.